Journal of Solid State Chemistry 183 (2010) 322–326

Contents lists available at ScienceDirect

Journal of Solid State Chemistry

journal homepage: www.elsevier.com/locate/jssc

Raman characterization of α- and β-$LiFe_5O_8$ prepared through a solid-state reaction pathway

W. Cook *, M. Manley

Department of Chemical Engineering, University of New Brunswick, 15 Dineen Drive, Fredericton, NB, Canada E3B 5A3

ARTICLE INFO

Article history:
Received 4 August 2009
Received in revised form
29 October 2009
Accepted 9 November 2009
Available online 13 November 2009

Keywords:
Lithium ferrite
Raman characteristion
Phase transformation

ABSTRACT

Lithium ferrite, a mixed-inverse spinel of type $A_xB_y[A_{1-x}B_{1-y}]O_4$ was produced through solid state synthesis by calcining a Li_2CO_3/Fe_2O_3 mixture at 900 °C. The presence of both the ordered α-phase and disordered β-phase of $LiFe_5O_8$ was confirmed by XRD analysis, while formation of the latter was achieved by air quenching from high temperature. Laser Raman analysis was performed on both the α-$LiFe_5O_8$ and β-$LiFe_5O_8$ powders in order to achieve a reference set of Raman shifts for the spinel. The strongest, characteristic Raman peaks were determined to be 493, 382, 358, 300, and 263 cm^{-1} for both phases while smaller peaks at 202 and 236 cm^{-1} present in the α-phase were diminishing in intensity when the β-phase was present, thus providing unique identifiers for the presence of the disordered ferrite structure. SEM images taken of the synthesized $LiFe_5O_8$ powders showed particle sizes of less than 300 nm and an even particle size distribution.

1. Introduction

Reactions with lithium-containing compounds have become an increasingly popular research topic with the continuing demand for advancement in lithium-ion battery technology and the need for new and longer lived energy sources. This has led to development of synthesis techniques and new applications of lithium compounds to act as the anode or cathode in lithium batteries. One possible lithium containing compound that has not received much attention is the transition-metal oxide lithium-ferrite ($LiFe_5O_8$). Potential uses of lithium ferrite are as a cathode material in rechargeable lithium batteries and as a cheaper alternative to garnet materials in microwave frequency studies [1]. Lithium ferrite is considered as a promising cathode material due to its low environmental impact [2] and lower cost compared to other commonly used materials such as Ni and Co [3]. Lithium ferrite can be used as a magnetic storage device due to its magnetic properties inherent in its cubic spinel structure [4].

Lithium ferrite ($LiFe_5O_8$ or $Li_{0.5}Fe_{2.5}O_4$) is an oxide with high saturation magnetization and a high Curie temperature. The crystal structure of β-$LiFe_5O_8$ has been compared to the inverse spinel structure of magnetite, Fe_3O_4, where half the ferric ions and the lithium ions occupy the octahedral interstices, the other half of the ferric ions occupy the tetrahedral interstices [5]. A typical spinel structure of the type AB_2O_4 contains a closed-packed cubic array of oxygen atoms, and only half of the octahedral and one eighth of the tetrahedral spaces are occupied. The unit cell consists of eight molecules. The 32e positions of space group Fd3m are occupied by the oxygen ions. In the AB_2O_4 structure, the B cations occupy the octahedral sites and the A cations occupy the 8a tetrahedral interstices. However, since each 8a tetrahedral site shares a face with four neighboring and empty 16c octahedral sites, there is a diffusion path for the A cations from 8a to 16c. Conversely, the 8b tetrahedral sites share common faces with 16d octahedral sites that are occupied by B cations, making their energy unsuited for cation occupation. An inverse and mixed spinel has the general formula $B[AB]O_4$ and $A_xB_y[A_{1-x}B_{1-y}]O_4$. Lithium ferrite fits the mixed spinel formula $Fe[Li_{0.5}Fe_{1.5}]O_4$, or $LiFe_5O_8$ [6].

In the ordered α-phase of $LiFe_5O_8$, the lithium and ferric ions are ordered in a 1:3 molar ratio in the octahedral sites of the cubic structure [7]. The disordered β-phase of lithium ferrite has a disordered face centered cubic structure where the lithium and ferric ions are randomly located in the octahedral interstices [2]. The disordered phase is produced with quenching from high temperatures as it is formed and prevalent in the temperature range of 750–1000 °C. Presumably, this is due to the relative diffusion rates of the ions in the cubic lattice. Slow cooling allows redistribution and ordering of the ions in the cubic lattice and provides the condition for the reversion to the ordered phase [7]. The disordered phase (β-$LiFe_5O_8$) is a good electric conductor and has reproducible conductivity between 22 and 850 °C. Its good conductivity is due to its n-type semiconductor properties as well as the considerable mobility of the lithium and ferric ions in the

* Corresponding author. Fax: +1 506 453 3591.
E-mail addresses: wcook@unb.ca (W. Cook), m.manley@unb.ca (M. Manley).

0022-4596/$ - see front matter © 2009 Elsevier Inc. All rights reserved.
doi:10.1016/j.jssc.2009.11.011

cubic, spinel matrix [8]. The ordered, α-phase of lithium ferrite has a variable conductivity below 740 °C when numerous samples are tested, showing that the ordered phase is not nearly as good a semiconductor as the disordered phase due to the immobility and ordering of the cations in the cubic structure [8].

The β-phase (disordered) of $LiFe_5O_8$ desired for production in this work can be produced through the following reaction:

$$2Fe_2O_3 + LiFeO_2\ (\alpha \text{ and } \beta) \rightarrow LiFe_5O_8\ (\beta) \quad (1)$$

The reaction must occur between 700 and 1000 °C and subsequently quenched in air for the β-phase to be produced and maintained. Calcination temperatures in excess of 1000 °C can promote irreversible lithium loss in the ferrite [9], however, calcination at or slightly above 1000 °C can promote the production of the α-phase of $LiFe_5O_8$ [10]. Phase transformation from α to β also occurs in the range of 740 ± 5 °C as the Fe_2O_3/Li_2CO_3 mixture is heated [8]. It is within this temperature range that, upon slow cooling, the β-phase will revert back to the α-phase thus, the β-phase must be sustained by quenching. The phase transformation at ~740 °C is likely due to the increased mobility of the lithium cation in the interstices due to increased diffusion rates and growing hole spacing in the crystal structure as the temperature is increased. The mobility of the lithium and ferric cations in the lattice, coupled with increased diffusion rates and mobility, creates the disorder in the crystal structure. The re-ordering of the ions above 1000 °C could be related to irreversible lithium loss caused by volitization of lithium at these higher temperatures [9]. The lithium and ferric ions diffuse into an ordered structure to achieve stability.

The electrical properties of $LiFe_5O_8$ are dependent on the synthesis route, grain size, composition of the sample, sintering temperature and atmosphere of testing (air saturated, inert, etc.). Permittivity's in ferrites, in general, are proportional to the square root of the conductivity so the grains have a higher conductivity and permittivity than the grain boundaries. Dielectric permittivity increases slowly with increase in temperature at lower temperatures, approximately up to 373 K. Above 373 K, permittivity increases rapidly [11]. The resistivity of ferrites decreases with increasing temperature, as ferrites are considered to be magnetic semiconductors. Dielectric permittivity is inversely proportional to the square of the resistivity [11].

There are many methods described in the literature to produce $LiFe_5O_8$ depending on the desired particle size. Some of these methods include: *low external temperature* [12]; *solid state reaction* (*the technique chosen for this work*) [8]; *freeze-drying* [13]; *self-combustion* [14]; *pulsed laser deposition technique* [15]; *hydro-thermal ball milling* [16]; *autocombustion* [7]; *microwave induced combustion process* [17]; *solid state formation from mechanically activated mixtures* [18]; *citrate precursor* [19]; *sol–gel synthesis* [1]; *flux methods* [20]; *double sintering ceramics* [21] and; *self propagating high temperature synthesis* [22].

Many of these synthesis techniques are more complicated than the one chosen in this work, calcination. The synthesis methods reviewed are typically used to produce a more refined product requiring many reactants and process steps. In some cases, gases such as NH_3 are evolved [12], which need to be specially handled. The method used here for $LiFe_5O_8$ synthesis was chosen because it is a simple and efficient way to produce a large sample of β-phase $LiFe_5O_8$ with little to no harmful off-gases or multiple-step chemical additions.

A method of solid state synthesis of lithium ferrite is proposed involving the simple reaction between lithium carbonate, Li_2CO_3, and hematite, Fe_2O_3. At temperatures between 400 and 1000 °C, carbon dioxide is evolved from the decomposition of the carbonate and lithium-iron oxide combines with excess hematite to form lithium ferrite [9]. Based on the literature review presented above, air quenching from above 750 °C should sustain the disordered β-phase of $LiFe_5O_8$.

The reaction mechanism proposed for the production of $LiFe_5O_8$ is a two-step reaction pathway with the initial step being the decomposition of the lithium carbonate to lithium-iron oxide, followed by the solid state combination and reordering of the lithium-iron oxide and hematite to form the lithium ferrite. The reactions would proceed as follows:

$$Li_2CO_3 + Fe_2O_3 \rightarrow 2LiFeO_2 + CO_2 \quad (2)$$

$$LiFeO_2 + 2Fe_2O_3 \rightarrow LiFe_5O_8 \quad (3)$$

This scheme has been proposed after a review of thorough thermogravimetric measurements and XRD [9]. Li_2CO_3 decomposes at temperatures above 400 °C, but above 700 °C the loss of Li^+ and O^{-2} from the ferrite, combined with a difference in density, allows the combination of $LiFe_5O_8$ into the β-spinel matrix [9,10].

2. Experimental

Lithium carbonate powder (Li_2CO_3 from Sigma-Aldrich: CAS 554-13-2, 99+%) was mixed with fine hematite powder (Fe_2O_3 from Fisher: CAS 1309-37-1, 99+%) in a 1:5 molar ratio, and the two components were ground with a ceramic mortar and pestle for 30 min. The 1:5 molar ratio of lithium carbonate to hematite is necessary to ensure that the second reaction in the mechanism shown in Eqs. (2) and (3) reaches completion.

Ethanol is added to the powder mixture to ensure homogeneity and is ground with the mortar until all of the ethanol is evaporated. The lithium-carbonate/hematite mixture was placed in three separate ceramic crucibles to compare the effect of cooling rates on the final composition. All three crucibles were heated to 900 °C at a rate of 33 °C/h to allow slow decomposition of Li_2CO_3 [9]. After 3 h at 900 °C, the heater was shut off. One crucible was left to slow cool in the furnace for 24 h, while the other two were removed to quench in air. To compare quenching rates, the powder from one of the crucibles was poured onto a ceramic plate and broken up to promote increased heat transfer and cooling while the other was left to air-quench in the crucible without being disturbed. The powders were collected in vials and stored.

Following the sample preparation, the powders were collected and characterized by scanning electron microscopy (SEM), X-ray diffraction (XRD), laser Raman microscopy and electron diffraction in a transmission electron microscope (TEM). A JEOL, JSM6400 digital SEM with Gellar dPict digital image acquisition software was used for the SEM work. For the XRD, the X-ray source was a 2.2 kW Cu X-ray tube with an operating power and current of 40 kW and 30 mA, respectively. X-ray optics used were the standard Bragg–Brentano para-focusing mode. A step size of 0.02° and 1.0 s were used during the testing. A Pelletier-cooled solid state (Si [Li]) detector (Sol-X) with a useful energy range of 1.60 keV was employed. Raw data was analyzed with the EVA program. For the Raman characterization, a Renishaw inVia Raman microscope was employed. The microscope uses a He–Ne gas mixture @ 633 nm, which is considered to be a mid-range wavelength. The TEM electron diffraction patterns were taken using a JEOL 2011 STEM with Gatan imaging filter (GIF 2000), Gatan 4 k × 4 k Ultrascan digital camera, and atomic structure –Z–contrast imaging (HAADF). The JEOL 2001 also used energy filtered TEM (EFTEM).

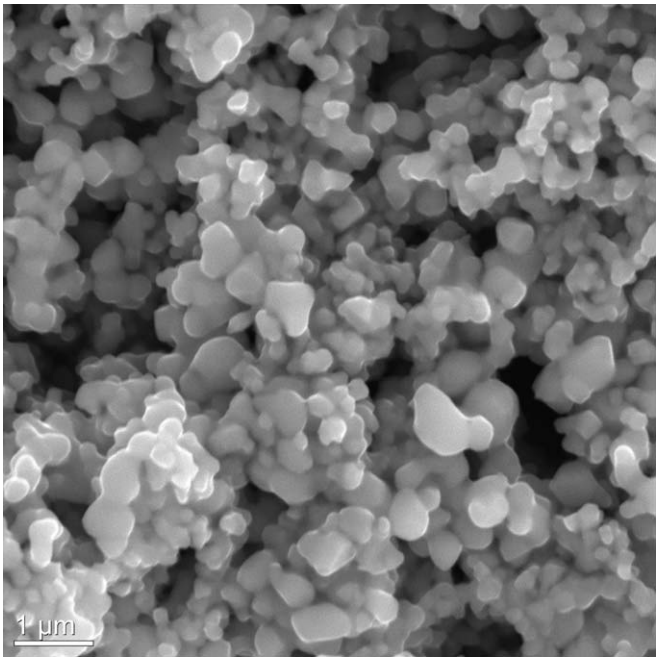

Fig. 1. SEM image showing even particle distribution in β-$LiFe_5O_8$ powder and average particle size less than 300 nm.

3. Results

The powder collected from the quenched samples, expected to include the β-phase of $LiFe_5O_8$, was reddish-brown in appearance and occupied approximately the same volume in the crucible, although it could be seen that some contraction had occurred since the bulk of the sample had rescinded from the crucible walls.

Imaging was completed by scanning electron microscopy (SEM) to view the particles and particle size distribution of the quenched lithium ferrite powder produced through this simple solid-state synthesis route. The resulting images showed the particles are 300 nm or less in diameter and have a fairly even particle size distribution (see Fig. 1 as an example).

The powder was taken and analyzed using XRD to characterise the products and phases present. The XRD results are shown in Fig. 2(a–c) with the baseline peaks expected for both the alpha and beta phases.

The powder was then sent to retrieve baseline peaks for lithium ferrite (ordered and disordered phases) with the Laser Raman microscope. The baseline Raman peaks for the ordered and disordered lithium ferrites are shown in Figs. 3 and 4.

Diffraction patterns and diffraction angles were determined in a TEM by transmission electron spectroscopy to further confirm the presence of the β-$LiFe_5O_8$ phase. Fig. 5 shows the electron diffraction pattern obtained from the air-quenched then spread lithium ferrite sample.

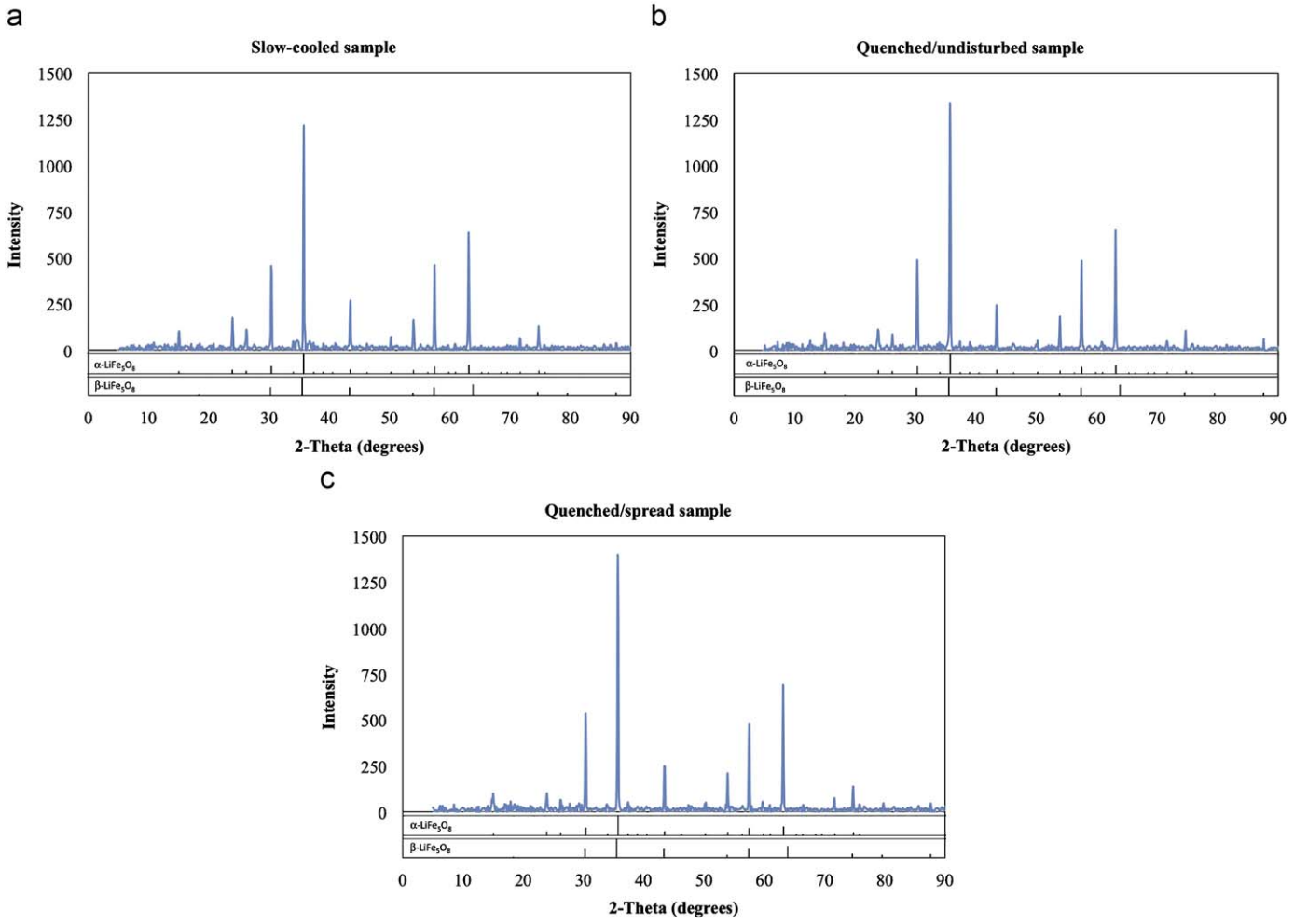

Fig. 2. (a) XRD spectrum of the slow-cooled powder. (b) XRD spectrum of the undisturbed air-quenched powder. (c) XRD spectrum of the air-quenched and spread powder.

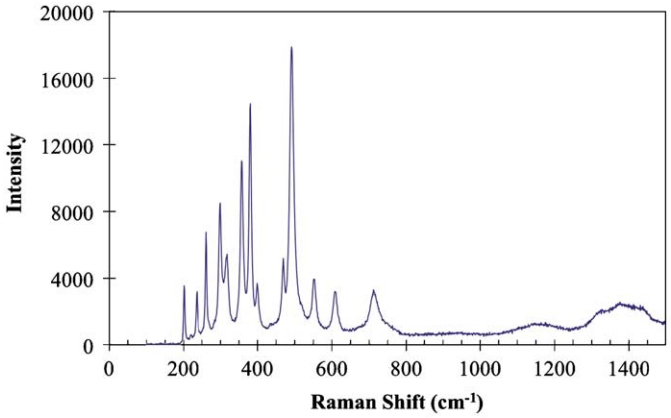

Fig. 3. Laser Raman spectrum for α-phase lithium ferrite.

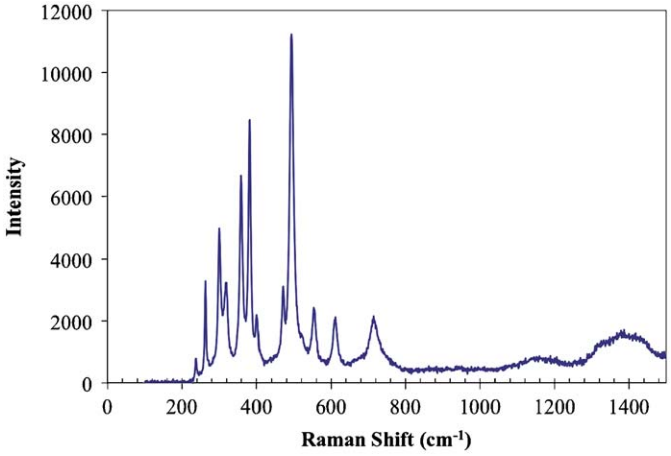

Fig. 4. Laser Raman spectrum for β-phase lithium ferrite.

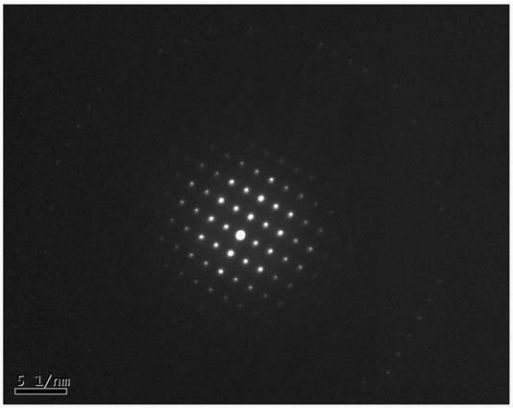

Fig. 5. TEM electron diffraction pattern of the air-quenched and spread powder.

4. Discussion

The XRD spectrum, shown in Fig. 2(a–c), confirms that that powder produced did indeed contain a significant portion of the disorderd β-phase of $LiFe_5O_8$. As there are few distinguishing peaks for the β-phase compared with the α-phase, one must look at the diminishing proportions of two supplementary peaks that are present for the α-phase to confirm the presence of the β-phase in the bulk sample. The slow-cooled powder produced purely α-phase $LiFe_5O_8$, seen in Fig. 2(a). The peaks at 23.8°, 26.2° (offset by 5°) and 50.5° are clearly diminished in Fig. 2(b), the XRD graph of the air-quenched but undisturbed powder. The lower end peaks are even further diminished for the air-quenched and distributed powder—Fig. 2(c) as the powder was more quickly quenched, preserving more of the disordered phase. By comparing the slow-cooled graph, the quenched/undisturbed graph and the quenched/spread graph, we see the proportions between the peaks at diffractions angles 35.8°, 23.8° and 26.2° (as determined by differences in the relative peak heights) decrease from 0.147 and 0.092 in the pure α-phase powder to 0.0889 and 0.0556 in the quenched/undisturbed powder and to 0.072 and 0.045 in the quenched/spread powder. The peak at 35.8° is used as a reference as it is the strongest peak in common with both α and β phases. Assuming the slow-cooled powder is purely α-phase, this corresponds to approximately 38% β-phase formed in the undisturbed powder between 50% and 55% β-phase retained in the quenched/spread powder.

Table 1
Primary Laser Raman peaks for α- and β-phase lithium-ferrite in decreasing order of intensity.

Peak	Raman shift (cm^{-1})
1	493
2	382
3	358
4	300
5	263
6	318
7	469
8	553
9	400
10	201[a]
11	716
12	610
13	236[a]

[a] Peaks not expected to be present in pure β-$LiFe_5O_8$.

The Raman characterization of the α-phase $LiFe_5O_8$ in Fig. 3 clearly exhibits peaks in the 200–250 cm^{-1} region, one of which at 202 cm^{-1} that is not visible on the Raman scan of the predominately β-phase ferrite in Fig. 4. The other low-end peak, at 236 cm^{-1}, is clearly diminished in the sample containing the β-phase indicating a significantly reduced fraction of α-phase in the sample. The main peaks identifying α- and β-$LiFe_5O_8$ by the Laser Raman analysis are listed in Table 1. Of note is the absence of the peak at 202 cm^{-1} when the β-phase is present and the shrinking intensity of the peak at 236 cm^{-1}. Presumably, in a pure β-$LiFe_5O_8$ sample, both these peaks would vanish.

To further confirm that β-$LiFe_5O_8$ was indeed present, TEM diffraction patterns were obtained for the air-quenched then spread powder. Fig. 5 shows the electron diffraction pattern produced. The resulting d-spacing measurements showed that there was a degree of disorder within the sample. The longest characteristic d-spacing is 4.84 Å for β-$LiFe_5O_8$, and 5.89 Å for α-$LiFe_5O_8$ according to the JCPDS-ICDD database used for the TEM referencing software (alpha phase #38-259; beta phase #17-114). Various spots measured on the grain showed d-spacings of 4.88 and 5.92 Å, therefore, the sample must contain both ordered and disordered lithium ferrite. A pure sample of α-$LiFe_5O_8$ would not contain any d-spacings in the range of 4.8 Å as is shown in the JCPDS.

5. Conclusions

Synthesis of lithium ferrite was investigated for the purpose of determining identifiable peaks by Laser Raman analysis and to

provide a distinction between the ordered (α) and disordered (β) phases. It was found that by combining lithium carbonate powder with fine hematite powder in a 1:5 molar ratio, heating the well-blended mixture in air at 900 °C for 3 h and air quenching to room temperature, a bulk sample containing greater than 50% of the β-phase lithium-ferrite powder could be simply produced. SEM images of the β-$LiFe_5O_8$ powder showed particles less than 300 nm in diameter with an even particle distribution.

The composition of the powder was confirmed by XRD analysis to be pure lithium ferrite ($LiFe_5O_8$) containing a significant amount of the desired β-phase (between 38% and 55%), the proportion increasing with faster quenching from high temperature. The various forms of the lithium-ferrite powder were analyzed by Laser Raman spectroscopy to provide a reference set of peaks identifying the different lithium-ferrite phases. The largest peaks resulting from the Raman analysis were found to be 493, 382, 358, 300, and 263 (shift, cm^{-1}). The peaks at 202 and 236 cm^{-1} are present for the α-phase powder but disappear when considerable β-phase is present; thus, providing a clear indicator for the presence of β-$LiFe_5O_8$.

TEM diffraction patterns further confirm the presence of β-$LiFe_5O_8$. The d-spacing measurement of the air-quenched then spread sample of lithium ferrite contained characteristic d-spacing of both α- and β-$LiFe_5O_8$, represented by 5.92 and 4.84 Å, respectively.

Acknowledgments

The authors wish to express their gratitude towards NSERC for financial support of this study. We are also grateful to Dr. Louise Weaver and Dr. Steve Cogswell for TEM and XRD analysis, Dr. Lihui Liu for Laser Raman characterization and Dr. Douglas Hall for SEM imaging.

References

[1] S.Y. An, I.-B. Shim, C.S. Kim, Journal of Magnetism and Magnetic Materials 290–291 (2004) 1551.
[2] S. Wang, L. Gao, L. Li, H. Zheng, Z. Zhang, W. Yu, Y. Qian, Institute of Physics Publishing—Nanotechnology 16 (2005) 2677.
[3] M. Tabuchi, K. Ado, H. Sakaebe, C. Masquelier, H. Kageyama, O. Nakamura, Solid State Ionics 79 (1995) 220.
[4] S. Dey, A. Roy, D. Das, J. Ghose, Journal of Magnetism and Magnetic Materials 270 (2004) 224.
[5] M.P. Bogdanovich, Soviet Physics-Solid State 32 (1990) 3.
[6] C.J. Chen, M. Greenblatt, Journal of Solid State Chemistry 64 (1986) 240.
[7] S. Verma, J. Karande, A. Patidar, P.A. Joy, Materials Letters 59 (2005) 2630.
[8] T. Matsui, J.B. Wagner Jr., Journal of The Electrochemical Society 124 (1977) 1141.
[9] A.J. Pointon, R.C. Saull, Journal of the American Ceramic Society 52 (1969) 157.
[10] G.A. El-Shabaky, A.A. Ibrahim, Thermica Acta 118 (1987) 151.
[11] M.R. Anantharaman, M. George, A.M. John, P.A. Joy, S.S. Nair, Journal of Applied Physics 39 (2006) 900.
[12] S. Uzunova, I. Uzunov, D. Kovacheva, A. Momchilov, B. Puresheva, Journal of Applied Electrochemistry 36 (2006) 1333.
[13] A. Hiraki, T. Ito, S. Koizumi, H. Okajima, M. Suzuki, T. Tachiwaki, Applied Surface Science 70 (1992) 751.
[14] P.D. Popa, E. Rezlescu, N. Rezlescu, Journal of Magnetism and Magnetic Materials 272–276 (2004) e1811.
[15] G. Balestrino, S. Martellucci, A. Paoletti, P. Paroli, G. Petrocelli, A. Tebano, Solid State Communications 96 (1995) 997.
[16] A. Ahniyaz, T. Fujiwara, S. Song, M. Yoshimura, Solid State Ionics 151 (2002) 419.
[17] Y. Fu, C. Lin, C. Liu, Y. Yao, Journal of Alloys and Compounds 395 (2004) 247.
[18] V. Berbenni, A. Marini, P. Matteazzi, R. Ricceri, N.J. Welham, Journal of European Ceramic Society 23 (2002) 527.
[19] D.P.E. Dickson, C.E. Johnson, Q.A. Pankhurst, V.K. Sankaranarayanan, Journal of Magnetism and Magnetic Materials 130 (1993) 288.
[20] Z.C. Xu, Journal of Applied Physics 93 (2003) 4746.
[21] L. Radhapiyari, S. Phanjoubam, H.N.K. Sarma, C. Prakash, Materials Letters 44 (2000) 65.
[22] M.V. Kuznetsov, Q.A. Pankhurst, I.P. Parkin, Journal of Applied Physics 31 (1998) 2886.